

A new measurement of the antiproton-to-proton flux ratio up to 100 GeV in the cosmic radiation

O. Adriani,^{1,2} G. C. Barbarino,^{3,4} G. A. Bazilevskaya,⁵ R. Bellotti,^{6,7} M. Boezio,⁸ E. A. Bogomolov,⁹ L. Bonechi,^{1,2} M. Bongi,² V. Bonvicini,⁸ S. Bottai,² A. Bruno,^{6,7} F. Cafagna,⁷ D. Campana,⁴ P. Carlson,¹⁰ M. Casolino,¹¹ G. Castellini,¹² M. P. De Pascale,^{11,13} G. De Rosa,⁴ D. Fedele,^{1,2} A. M. Galper,¹⁴ L. Grishantseva,¹⁴ P. Hofverberg,¹⁰ A. Leonov,¹⁴ S. V. Koldashov,¹⁴ S. Y. Krutkov,⁹ A. N. Kvashnin,⁵ V. Malvezzi,¹¹ L. Marcelli,¹¹ W. Menn,¹⁵ V. V. Mikhailov,¹⁴ M. Minori,¹¹ E. Mocchiutti,⁸ M. Nagni,¹¹ S. Orsi,¹⁰ G. Osteria,⁴ P. Papini,² M. Pearce,¹⁰ P. Picozza,^{11,13} M. Ricci,¹⁶ S. B. Ricciarini,² M. Simon,¹⁵ R. Sparvoli,^{11,13} P. Spillantini,^{1,2} Y. I. Stozhkov,⁵ E. Taddei,^{1,2} A. Vacchi,⁸ E. Vannuccini,² G. Vasilyev,⁹ S. A. Voronov,¹⁴ Y. T. Yurkin,¹⁴ G. Zampa,⁸ N. Zampa,⁸ and V. G. Zverev¹⁴

¹*Physics Department of University of Florence,
I-50019 Sesto Fiorentino, Florence, Italy*

²*INFN, Sezione di Florence, I-50019 Sesto Fiorentino, Florence, Italy*

³*Physics Department of University of Naples "Federico II", I-80126 Naples, Italy*

⁴*INFN, Sezione di Naples, I-80126 Naples, Italy*

⁵*Lebedev Physical Institute, RU-119991 Moscow, Russia*

⁶*Physics Department of University of Bari, I-70126 Bari, Italy*

⁷*INFN, Sezione di Bari, I-70126 Bari, Italy*

⁸*INFN, Sezione di Trieste, I-34012 Trieste, Italy*

⁹*Ioffe Physical Technical Institute, RU-194021 St. Petersburg, Russia*

¹⁰*Royal Institute of Technology (KTH),
Department of Physics, SE-10691 Stockholm, Sweden*

¹¹*INFN, Sezione di Rome "Tor Vergata", I-00133 Rome, Italy*

¹²*IFAC, I-50019 Sesto Fiorentino, Florence, Italy*

¹³*Physics Department of University of Rome "Tor Vergata", I-00133 Rome, Italy*

¹⁴*Moscow Engineering and Physics Institute, RU-11540 Moscow, Russia*

¹⁵*Physics Department of Universität Siegen, D-57068 Siegen, Germany*

¹⁶*INFN, Laboratori Nazionali di Frascati, I-00044 Frascati, Italy*

(Dated: February 25, 2009)

Abstract

A new measurement of the cosmic ray antiproton-to-proton flux ratio between 1 and 100 GeV is presented. The results were obtained with the PAMELA experiment, which was launched into low-earth orbit on-board the Resurs-DK1 satellite on June 15th 2006. During 500 days of data collection a total of about 1000 antiprotons have been identified, including 100 above an energy of 20 GeV. The high-energy results are a ten-fold improvement in statistics with respect to all previously published data. The data follow the trend expected from secondary production calculations and significantly constrain contributions from exotic sources, e.g. dark matter particle annihilations.

PACS numbers: 96.50.sb, 95.35.+d, 95.55.Vj

Antiprotons can be produced from collisions of energetic cosmic ray particles, primarily protons, with the constituents of the interstellar gas such as hydrogen and helium. Possible primary sources of galactic antiprotons include the annihilation of dark matter particles [1, 2] and the evaporation of primordial black holes [3, 4]. Cosmic ray antiproton experiments can probe production and transport properties of cosmic rays in the galaxy and search for evidence of exotic production mechanisms. However, such detailed studies of the antiproton energy spectrum require measurements with good statistics over a large energy range. Cosmic ray antiprotons were first observed in pioneering experiments in the 1970s by Bogomolov et al. [5] and Golden et al. [6] using balloon-borne magnetic spectrometers. Bogomolov et al. observed 2 antiprotons in the kinetic energy range 2-5 GeV while Golden et al. observed 28 antiprotons in the range 5-12 GeV. Several other experiments followed, covering the kinetic energy range 0.2-50 GeV. More than 1000 antiprotons have been observed in the kinetic energy range 0.2-4 GeV by the BESS experiment [7] while the statistics at higher energies is very limited. The CAPRICE98 [8], HEAT [9] and MASS91 [10] balloon-borne experiments have observed a total of about 80 antiprotons above 5 GeV. However, only two cosmic ray antiprotons with a kinetic energy above 30 GeV are reported [8].

The antiproton-to-proton flux ratio has been measured from 1 to 100 GeV by the PAMELA experiment (a Payload for Antimatter Matter Exploration and Light-nuclei Astrophysics), a satellite-borne apparatus designed to study charged particles in the cosmic radiation with a particular emphasis on antiparticles. The statistics, particularly at high energies, is significantly increased compared to the total data sets provided by all previous experiments.

The PAMELA apparatus is inserted inside a pressurized container (2 mm aluminum window) attached to the Russian Resurs-DK1 satellite and comprises the following subdetectors: a time of flight system (ToF); a magnetic spectrometer; an anticoincidence system (AC); an electromagnetic imaging calorimeter; a shower tail catcher scintillator and a neutron detector. Technical details about the entire PAMELA instrument and launch preparations can be found in [11].

PAMELA has been acquiring data since July 11th 2006. The results presented in this letter refer to data acquired in the period July 2006 to February 2008. More than one billion triggers have been collected during the total acquisition time of ~ 500 days. Events were considered for further analysis if the reconstructed rigidity exceeded the vertical geomagnetic

cut-off, estimated using the satellite position, by a factor of 1.3. Downward-going particles were selected using the ToF information. The time-of-flight resolution of 300 ps ensures that no contamination from albedo particles remains in the selected sample. The ionization losses (dE/dx) in the ToF scintillators and in the silicon tracker layers were used to select minimum ionizing singly charged particles. Furthermore, multiply charged tracks were rejected by requiring no spurious signals in the ToF and AC scintillators above the tracking system.

Particle identification is based on the determination of rigidity by the spectrometer and the properties of the energy deposit and interaction topology in the calorimeter. The analysis technique was validated using the PAMELA Collaboration’s official simulation program tuned using particle beam data.

The tracking information from the spectrometer is crucial for selecting antiprotons. Due to the finite spectrometer resolution, corresponding to a maximum detectible rigidity (MDR) exceeding 1 TV, high rigidity protons may be assigned the wrong sign of curvature. In addition there is a background from protons that scatter in the material of the tracking system and mimic the trajectory of negatively-charged particles. In order to accurately measure antiprotons, this “spillover” was eliminated by imposing a set of strict selection criteria on the quality of the fitted tracks. Track fits required the use of at least 4 (3) position measurements along the x (y) direction and an acceptable χ^2 for the fitted track. To remove spillover protons, clean tracking position measurements were required (e.g. no accompanying hits from delta-ray emission) and that the MDR, estimated for each event during the fitting procedure, should be 10 times larger than the reconstructed rigidity. The deflection ($1/\text{rigidity}$) distribution for positively- and negatively-charged down-going particles, which did not produce an electromagnetic shower in the calorimeter, is shown in Figure 1. The sample includes events for which the reconstructed MDR is larger than 850 GV. The good separation between negatively-charge particles and spillover protons is evident. As expected, the antiproton tracking requirements limit the distribution of spillover protons.

The calorimeter was used to reject electrons. The longitudinal and transverse segmentation of the calorimeter combined with dE/dx measurements from the individual silicon strips allow electromagnetic showers to be identified with very high accuracy. Using electrons from simulations and particle beams, and simulated antiprotons, we defined an energy dependent calorimeter antiproton selection [12]. Several topological calorimeter variables are used for

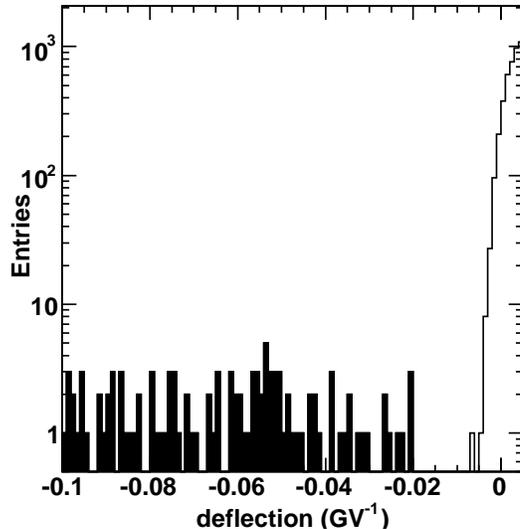


FIG. 1: The deflection reconstructed by the track fitting procedure for negatively- and positively-charged down-going particles with a reconstructed MDR ≥ 850 GeV and that did not produce an electromagnetic shower in the calorimeter. The shaded histogram corresponds to the selected antiprotons.

the antiproton identification. As an example, the energy density in the shower core weighted by the depth in the calorimeter, Q_{core}/N_{core} , is shown in Figure 2. The distribution for the proton-dominated positively-charged sample is peaked at 1.25. In the negatively-charged sample, the distribution corresponding to electrons peaks at a higher value, and antiproton events are collected in a separate peak positioned similarly to that seen in the positively-charged sample. The resulting electron contamination was estimated to be negligible across the whole energy range of interest. The different, and momentum dependent, interaction cross sections for protons and antiprotons were taken into account estimating the calorimeter selection efficiencies as a function of momentum for both species. These efficiencies were studied using both simulated antiprotons and protons, and proton samples selected from the flight data. In the rigidity interval 2 - 100 GV the proton selection efficiency ranges between 0.720 ± 0.003 and 0.800 ± 0.012 , whereas the antiproton efficiency ranges between 0.621 ± 0.003 and 0.797 ± 0.012 . These efficiencies were used to rescale the number of selected antiprotons and protons.

Possible contamination from pions produced by cosmic-ray interactions with the PAMELA payload was studied using both simulated and flight data. Both negatively-

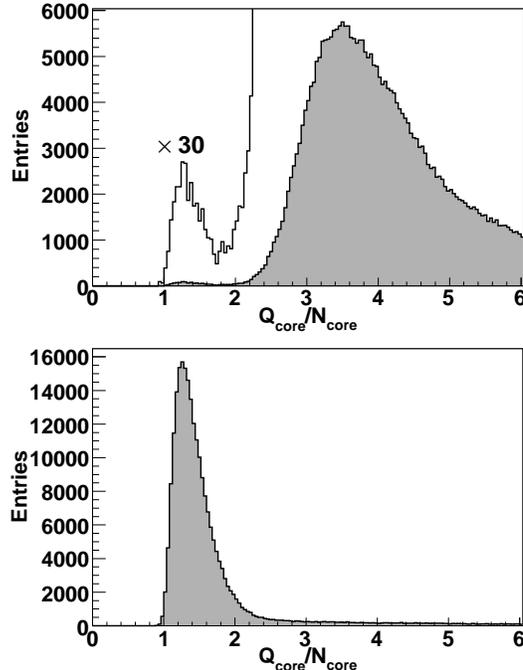


FIG. 2: An example of a topological calorimeter variable used for antiproton identification (see text for explanation). Positively-charged events are shown in the lower plot. The upper plot shows negatively-charged events. The vertical scale for the open histogram has been multiplied by a factor of 30 (compared to the filled histogram) for clarity.

and positively-charged pions below 1 GV were identified using the β (velocity) measured by the ToF system and the calorimeter information (to reject electrons and positrons). The majority of these pion events had hits in the AC scintillators and/or large energy deposits in one of the top ToF scintillator clearly indicating that they were the product of cosmic ray interactions with the PAMELA structure or pressure vessel. After applying all previously described selection criteria, the energy spectrum of the surviving pions was measured below 1 GV and compared with the corresponding spectrum obtained from simulation by using both GHEISHA and FLUKA generators [13, 14]. After comparison with the experimental pion spectrum below 1 GV, a normalization factor for the simulation, which accounted for all uncertainties related to pion production and hadronic interactions, was obtained. The normalized simulated pion spectrum was used to estimate the contamination in the antiproton sample for rigidities greater than 1 GV. This procedure resulted in a residual pion contamination of less than 5% above 2 GV, decreasing to less than 1% above 5 GV. This result was

TABLE I: Summary of proton and antiproton results.

Rigidity at spectrometer	Mean Kinetic Energy	Observed number of events		Extrapolated $\frac{\bar{p}}{p}$ at top of payload
GV	GeV	\bar{p}	p	
2.23 - 2.58	1.64	39	1198039	$(3.92 \pm 0.63) \times 10^{-5}$
2.58 - 2.99	1.99	48	1144014	$(4.92 \pm 0.71) \times 10^{-5}$
2.99 - 3.45	2.41	55	1071778	$(5.91 \pm 0.80) \times 10^{-5}$
3.45 - 3.99	2.89	60	988666	$(6.89 \pm 0.89) \times 10^{-5}$
3.99 - 4.62	3.46	74	903708	$(9.2 \pm 1.1) \times 10^{-5}$
4.62 - 5.36	4.13	71	827521	$(9.6 \pm 1.1) \times 10^{-5}$
5.36 - 6.23	4.91	93	738028	$(1.40 \pm 0.14) \times 10^{-4}$
6.23 - 7.27	5.85	78	653736	$(1.31 \pm 0.15) \times 10^{-4}$
7.27 - 8.53	6.98	69	573172	$(1.32 \pm 0.16) \times 10^{-4}$
8.53 - 10.1	8.37	67	505503	$(1.44 \pm 0.18) \times 10^{-4}$
10.1 - 12.0	10.1	94	449261	$(2.27 \pm 0.23) \times 10^{-4}$
12.0 - 14.6	12.3	58	405583	$(1.54 \pm 0.20) \times 10^{-4}$
14.6 - 18.1	15.3	58	301314	$(2.05 \pm 0.27) \times 10^{-4}$
18.1 - 23.3	19.5	46	270068	$(1.80 \pm 0.27) \times 10^{-4}$
23.3 - 31.7	25.9	39	211249	$(1.94 \pm 0.31) \times 10^{-4}$
31.7 - 48.5	37.3	24	136858	$(1.82 \pm 0.37) \times 10^{-4}$
48.5 - 100.0	61.2	6	57613	$(1.07^{+0.58}_{-0.39}) \times 10^{-4}$

cross-checked between 4 and 8 GV by selecting antiproton events below the geomagnetic cut-off. This sample includes re-entrant-albedo [23] antiprotons and locally produced pions. By scaling the number of such events for the acquisition time an upper limit for the negative pion (and protons with the wrong sign for the reconstructed deflection) contamination in the cosmic ray antiproton sample was found to be $\sim 3\%$, in agreement with simulations.

Table I shows the total number of antiprotons and protons that survived the data selection. The antiproton-to-proton flux ratio was corrected for the calorimeter selection efficien-

cies and for the loss of particles in the instrument itself. It is assumed that all antiprotons and protons interacting with the payload material above and inside the tracking system are rejected by the selection criteria. The resulting antiproton-to-proton flux ratios are given in Table I and Figures 3 and 4. The reported errors are statistical only. The contamination

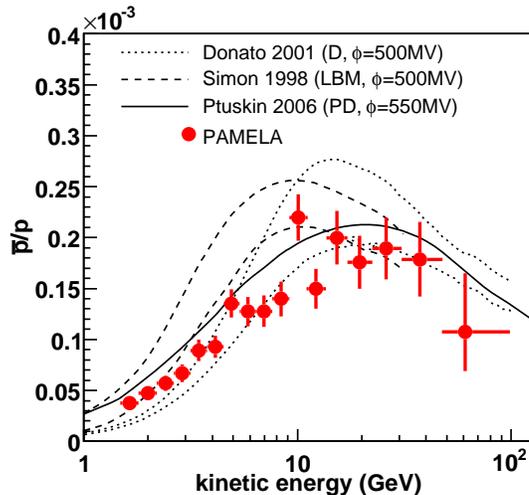


FIG. 3: The antiproton-to-proton flux ratio obtained in this work compared with theoretical calculations for a pure secondary production of antiprotons during the propagation of cosmic rays in the galaxy. The dashed lines show the upper and lower limits calculated by Simon et al. [15] for the standard Leaky Box Model, while the dotted lines show the limits from Donato et al. [16] for a Diffusion model with reacceleration. The solid line shows the calculation by Ptuskin et al. [17] for the case of a Plain Diffusion model. The curves were obtained using appropriate solar modulation parameters (indicated as ϕ) for the PAMELA data taking period.

was not subtracted from the results and should be considered as a systematic uncertainty. It is less than a few percent of the signal, which is significantly lower than the statistical uncertainty. Figure 3 shows the antiproton-to-proton flux ratio measured by the PAMELA experiment compared with theoretical calculations assuming pure secondary production of antiprotons during the propagation of cosmic rays in the galaxy. The PAMELA data are in excellent agreement with recent data from other experiments, as shown in Figure 4.

We have presented the antiproton-to-proton flux ratio over the most extended energy range ever achieved and we have improved the existing statistics at high energies by an order of magnitude. The ratio increases smoothly from about 4×10^{-5} at a kinetic energy of about 1 GeV and levels off at about 1×10^{-4} for energies above 10 GeV. Our results

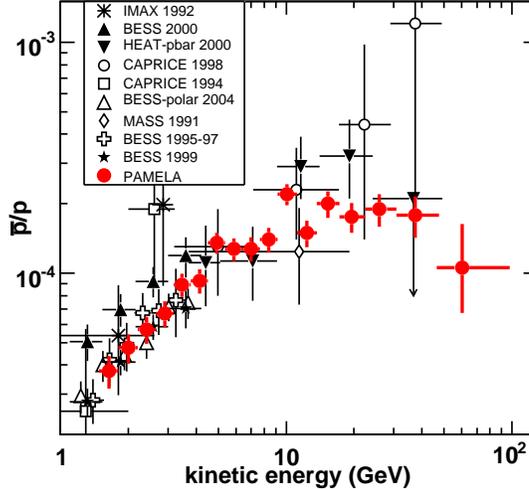


FIG. 4: The antiproton-to-proton flux ratio obtained in this work compared with contemporary measurements [8, 9, 10, 18, 19, 20, 21].

are sufficiently precise to place tight constraints on parameters relevant for secondary production calculations, e.g.: the normalization and the index of the diffusion coefficient, the Alfvén speed, and contribution of a hypothetical “fresh” local cosmic ray component [22]. Furthermore, an important test criteria for cosmic ray propagation models is their ability to reproduce both the antiproton-to-proton flux ratio and the secondary-to-primary nuclei ratio. Our high energy data (above 10 GeV) places limits on contributions from exotic sources, such as dark matter particle annihilations. The antiproton-to-proton flux ratio will be modified according to values of the dark matter particle mass, annihilation cross section, and structure in the density profile (boost factor).

PAMELA is continuously taking data and the mission is planned to continue until at least December 2009. The increase in statistics will allow higher energies to be studied. An analysis for low energy antiprotons (down to ~ 100 MeV) is in progress and will be the topic of a future publication [13].

We would like to acknowledge contributions and support from: Italian Space Agency (ASI), Deutsches Zentrum für Luft- und Raumfahrt (DLR), The Swedish National Space Board, Swedish Research Council, The Russian Space Agency (Roscosmos) and The Russian Foundation for Basic Research.

-
- [1] G. Jungman, M. Kamionkowski, and K. Griest, Phys. Rep. **267**, 195 (1996).
- [2] G. Bertone, D. Hooper, and J. Silk, Phys. Rep. **405**, 279 (2005).
- [3] S. Hawking, Nature **248**, 30 (1974).
- [4] P. Kiraly et al., Nature **293**, 120 (1981).
- [5] E. A. Bogomolov et al., in Proc. 16th Int. Cosmic Ray Conf. (Kyoto) (1979), vol. 1, p. 330.
- [6] R. L. Golden et al., Phys. Rev. Lett. **43**, 1196 (1979).
- [7] A. Yamamoto et al., Nucl. Phys. B (Proc. Suppl.) **166**, 62 (2007).
- [8] M. Boezio et al., Astrophys. J. **561**, 787 (2001).
- [9] A. S. Beach et al., Phys. Rev. Lett. **87**, 271101 (2001).
- [10] M. Hof et al., Astrophys. J. Lett. **467**, 33 (1996).
- [11] P. Picozza et al., Astropart. Phys. **27**, 296 (2007).
- [12] M. Boezio et al., Astropart. Phys. **26**, 111 (2006).
- [13] P. Hofverberg, Ph.D. thesis, Royal Institute of Technology, Stockholm (2008).
- [14] A. Bruno, Ph.D. thesis, University of Bari (2008).
- [15] M. Simon, A. Molnar, and S. Roesler, Astrophys. J. **499**, 250 (1998).
- [16] F. Donato et al., Astrophys. J. **563**, 172 (2001).
- [17] V. S. Ptuskin et al., Astrophys. J. **642**, 902 (2006).
- [18] J. Mitchell et al., Phys. Rev. Lett. **76**, 3057 (1996).
- [19] M. Boezio et al., Astrophys. J. **487**, 415 (1997).
- [20] Y. Asaoka et al., Phys. Rev. Lett. **88**, 051101 (2002).
- [21] T. Hams et al., in Proc. 30th Int. Cosmic Ray Conf. (Merida) (2006).
- [22] I. V. Moskalenko et al. Astrophys. J. **586**, 1050 (2003).
- [23] Secondary particles produced by cosmic rays interacting with the Earth's atmosphere that are scattered upward but lack sufficient energy to leave the Earth's magnetic field and re-enter the atmosphere in the opposite hemisphere but at similar magnetic latitude.